Chapter 13
BODIPY: A Unique Dye for Versatile Optical Applications

Soumyaditya Mula

13.1 Introduction

Fluorescent dyes are known for more than one and half a century, and still have the prime attraction to the scientists from multidisciplinary arena. They are the key elements in recent development of personal diagnostics, luminescent based organo-electronic devices and many other hi-tech applications. Thus, demand for the next-generation emissive dyes with tunable optical and electrical properties has increased. Countless classes of fluorescent organic dyes known so far vary in absorptivity and absorbance range, fluorescence colour and intensity, photo and chemical stability, triplet conversion rate etc. These are used for widespread hi-tech applications, such as laser dyes, chemical and bio-sensing, organic photovoltaics, OLEDs, cellular imaging as well as for other biological applications etc. (Valeur and Berberan-Santos 2012). Few of the most popular dyes are Rhodamine, pyrene, perylene, squaraine, cyanine, coumarin, boron-dipyrromethene (BODIPY), diketopyrrolo pyrrole (DPP), etc. (Fig. 13.1). Among these BODIPY (boradipyrromethene, 4,4-difluoro-4-bora-3a,4a-diaza-*s*-indacene) dyes have superior optical and redox properties. The first member of this class of compound was reported by Treibs and Kreuzer in 1968 (Treibs and Kreuzer 1968), although relatively little attention was given to the discovery until the end of the 1980s. After that, their potential applications were explored and the BODIPY dyes have been established as one of the most versatile fluorophores.

Structurally, BODIPY is a boron complex of dipyrromethene unit which can be considered as a "rigidified" monomethine cyanine dye (Fig. 13.1). This structural rigidification results unusually high fluorescence yields of the BODIPY core (Ulrich et al. 2008). The whole organic backbone is conjugated and extension of the conjugation is possible via attachment of different groups at various positions of one or both

S. Mula (✉)
Bio-Organic Division, Bhabha Atomic Research Centre, Mumbai 400085, India
e-mail: smula@barc.gov.in

Homi Bhabha National Institute, Anushakti Nagar, Mumbai 400094, India

R. S. Ningthoujam and A. K. Tyagi (eds.), *Handbook of Materials Science, Volume 1*,
Indian Institute of Metals Series, https://doi.org/10.1007/978-981-99-7145-9_13

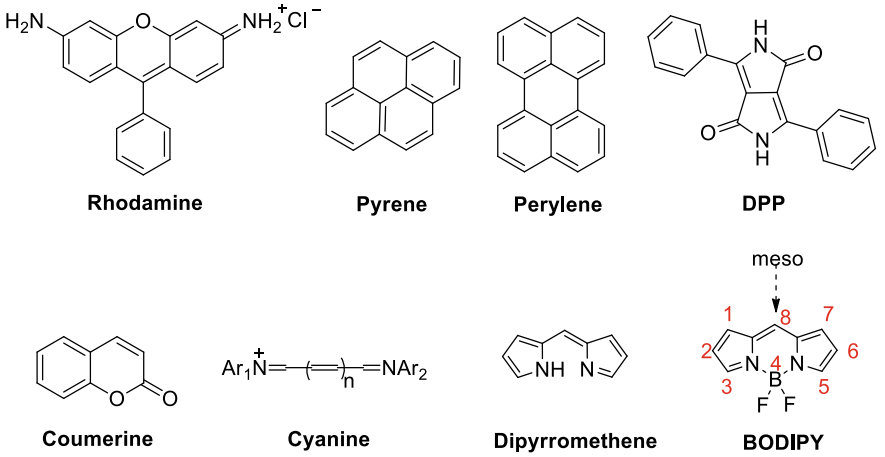

Fig. 13.1 Molecular structures of various organic dyes

pyrrole moieties. This helps to tune the fluorescence colour as well as the intensity of the moiety, which leads to countless numbers of tailored dyes for multiple applications (Mula et al. 2015; Gupta et al. 2013). Other properties such as high absorption coefficient, low triplet-state formation, good solubility in various organic solvents, excellent thermal and photochemical stability, and chemical robustness have made BODIPYs more attractive to the scientific fraternity (Mula et al. 2008).

13.2 Synthesis of BODIPY Dyes

Dipyrromethenes are synthesized by condensation of substituted/unsubstituted pyrroles with acid chlorides (aromatic/aliphatic)/acid anhydrides, or with acetals/aromatic aldehydes followed by oxidation using DDQ or p-chloranil. Then, BF_2-BODIPYs are synthesized by the complexation of corresponding dipyrromethenes with $BF_3.Et_2O$ in the presence of trialkylamine base (Et_3N or *i*-Pr_2NEt). Similarly, the dipyrromethenes can be reacted with BPh_3 to get the corresponding BPh_2-BODIPYs (Scheme 1) (Ulrich et al. 2008; Loudet and Burgess 2007; Mula et al. 2009). It is important to mention here that the *meso*-aryl/alkyl group can easily be chosen during the dipyrromethene synthesis which gives the possibility of synthesizing an array of BODIPY dyes with fluorescence in the UV–Vis region for different applications as discussed *vide infra*.

Aza-BODIPYs (4-bora-3a,4a,8-triazaindacene dyes) are very interesting as they have red shifted fluorescence in the far-red and near-IR region as compared to the conventional BODIPYs discussed above. Aza-dipyrromethenes are synthesized by reacting nitromethane with chalcone, followed by condensation with an ammonium salt (Scheme 2) (Ulrich et al. 2008; Loudet and Burgess 2007). Finally, complexation

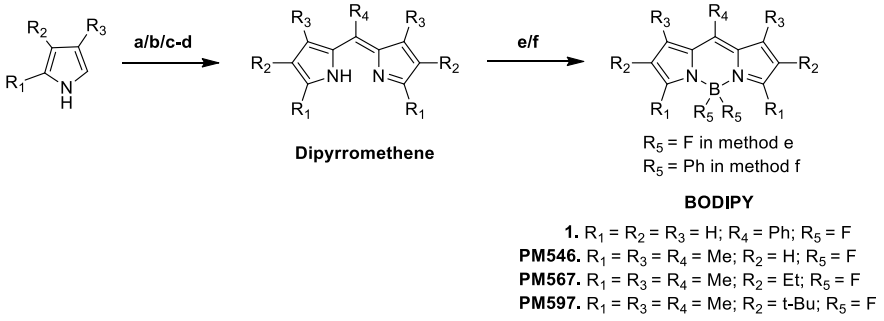

Scheme 1. Synthetic procedures for BODIPY dyes: **a** acid chloride/CH_2Cl_2/25 °C; **b** acid anhydride//25 °C; **c** acetal or aldehyde/TFA/CH_2Cl_2/25 °C; **d** *p*-chloranil or DDQ/CH_2Cl_2/25 °C; **e** Et_3N or *i*-Pr_2NEt/$BF_3.OEt_2$/CH_2Cl_2/25 °C; **f** BPh_3/toluene/90 °C

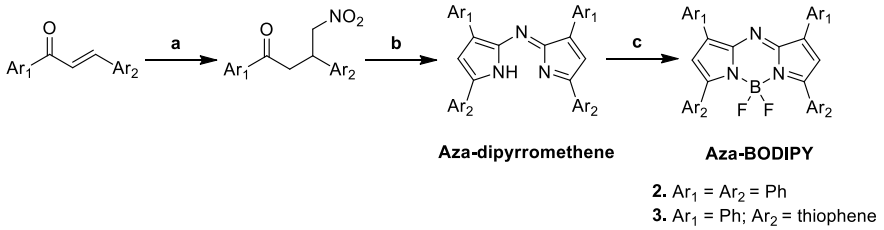

Scheme 2. Synthetic procedures for aza-BODIPY dyes: **a** CH_3NO_2, $HNEt_2$, MeOH, Δ; **b** NH_4OAc; **c** $BF_3{\cdot}OEt_2$, *i*-Pr_2NEt, rt

of aza-dipyrromethene with $BF_3{\cdot}OEt_2$ in the presence of *i*-Pr_2NEt furnished the corresponding BF_2-aza-BODIPYs.

13.3 Chemistry of BODIPY Core

13.3.1 Electrophilic Substitution at the Pyrrole Moiety

2,6-positions of the BODIPY core are the most reactive sites for the electrophilic substitutions. Treibs and Kreuzer first synthesized 2,6-disulfonic acid BODIPY dye by electrophilic substitution using chlorosulfonic acid (Treibs and Kreuzer 1968). This methodology was exploited later extensively to synthesize 2,6-dibromo/iodo/nitro/formyl BODIPYs which were subsequently used for further synthetic modifications (Scheme 3a) (Ulrich et al. 2008; Gupta et al. 2013; Loudet and Burgess 2007). Importantly, B-F bonds remain unaffected during these reactions and only 2,6-substituted products are obtained. Thus, this is an important synthetic methodology for regio-selective syntheses of functional BODIPYs. For example, water-solubility

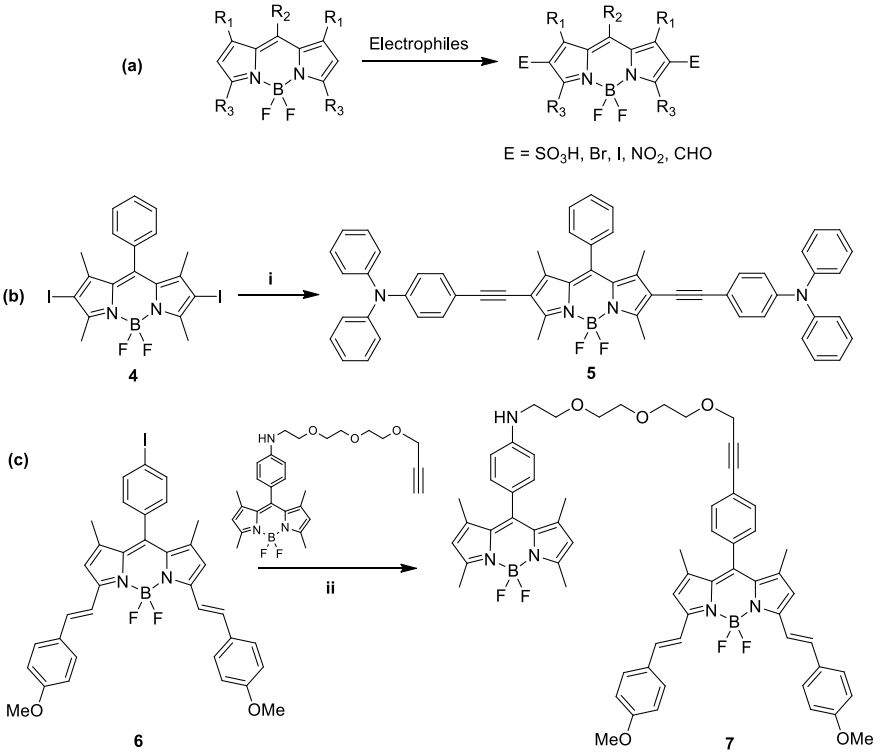

Scheme 3. **a** General procedure for eletrophilic substitution at 2,6 positions of BODIPY dyes: Electrophiles: $ClSO_3H$ or NBS or NIS or HNO_3 or $POCl_3$/DMF; **b** Synthesis of alkenyl BODIPY via Sonogashira coupling: (i) alkyne (2.5 equiv), $Pd(PPh_3)_4$, CuI, THF/NEt_3 (5:1), 60 °C; **c** Synthesis of BODIPY dyad: (ii) $[Pd(PPh_3)_4]$ (6 mol%), benzene, Et_3N, 50 °C

of the hydrophobic BODIPY dyes were increased by incorporation of the sulfonate groups keeping the absorption and emission profiles unchanged, whereas substitutions of nitro, bromo or iodo groups reduce the fluorescence drastically as compared to their parent dyes. The reduced fluorescence quantum yields of the bromo and iodo substituted BODIPYs is due to enhanced intersystem crossing (ISC) facilitated via the heavy-atom effect (Kamkaew et al. 2013), whereas nitro-BODIPYs are low/non-fluorescent due to Photoinduced Charge Transfer (PCT) discussed *vide infra.*

13.3.2 Metal-Mediated Cross-Coupling Reaction

Halogenated BODIPYs prepared from electrophilic substitutions discussed above or synthesized from halogen substituted pyrroles are very good precursors for different types of palladium-catalyzed coupling reactions such as Sonogashira, Suzuki, Heck

and Stille coupling (Scheme 3b-c). Interestingly, the B-F bonds remain unaffected during these cross-coupling reactions. These methodologies are extensively used to extent the conjugation length of the BODIPY chromophores and to build sophisticated dye structures with red shifted absorptions and emissions (Lu et al. 2014).

Additionally, 8-bromo/iodoaryl BODIPYs are used in similar kind of palladium-catalyzed cross-coupling reactions to connect with another aryl/heteroaryl fluorophore. The resultant multi component systems are used as efficient intermolecular electron and energy transfer molecular assemblies for hi-tech opto-electronic applications (Scheme 3c) (Mula et al. 2010).

13.3.3 Condensation at the Active Pyrrole-Methyl Groups

BODIPY dyes bearing methyl groups at 1, 3, 5, 7 and 8 positions are susceptible for the Knoevenagel type condensation reactions. These pyrrole methyl groups have higher acidity, thus deprotonate easily under mild conditions and the corresponding nucleophiles can be condensed with variety of aromatic aldehydes to synthesize styryl BODIPY dyes (Scheme 4). The reaction condition can be modulated to synthesize different regio-isomers and multi styryl BODIPY dyes with red shifted absorption and emission spectra. This methodology has been used extensively to develop functional BODIPYs emitting in the UV–Vis to NIR region for various applications (Lu et al. 2014; Shivran et al. 2011; Buyukcakir et al. 2009).

13.3.4 Modifications at the Boron Center

Substitution reactions at the boron center of the BODIPY dyes open the new arena of functionalized BODIPY dyes. Fluorine atoms at the B-center can be replaced using organometallic reagents (organolithium or Grignard reagents) to synthesize B-alkyl/aryl/ethynylaryl/ethynyl BODIPYs (Scheme 5) (Bodio and Goze 2019; Gupta et al. 2017; Jagtap et al. 2013). Due to the tetrahedral geometry of the B-center the substituents at the B-center do not have any direct electronic conjugation with the dipyrrin core. Thus, in contrast to the substitutions at the dipyrrin core, B-substitutions do not affect much the absorption and fluorescence wavelengths, but change the 3D structures of the molecules which helps to modify the other properties of the BODIPY dyes such as fluorescence quantum yield, redox properties, photo and chemical stability, solubility, aggregation behavior etc. The modifications at the B-center are highly useful for the preparing new dyads and cascade-type dyes molecules as discussed *vide infra.*

The boron substitutions reaction conditions with Grignard reagents were modified further to increase the yield and to reduce the reaction time. A typical reaction of BODIPY dye with EtMgBr furnished BEt_2-BODIPY with 67% yield in

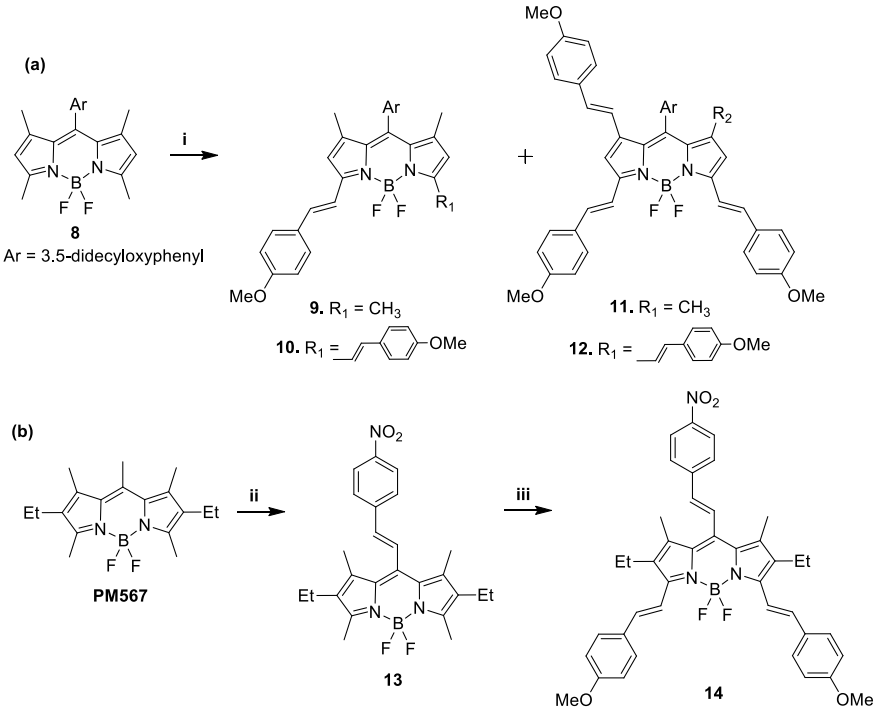

Scheme 4. General procedure for Knoevenagel type condensation reactions of BODIPY dyes: (i) *p*-anisaldehyde/AcOH/piperidine/PhH/Δ; (ii) *p*-nitrobenzaldehyde/AcOH/piperidine/toluene/Δ; (iii) *p*-anisaldehyde/AcOH/piperidine/toluene/Δ

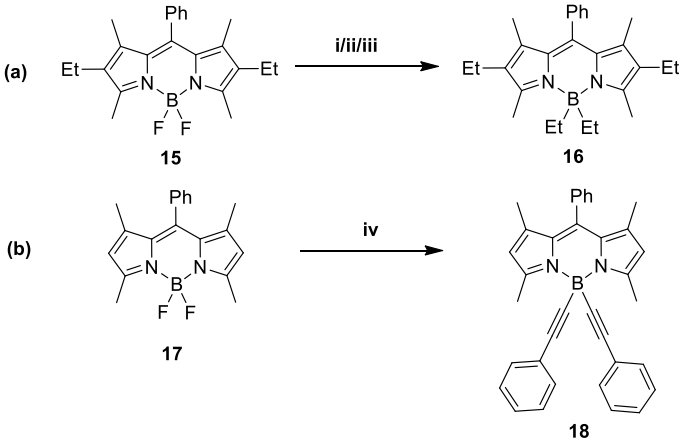

Scheme 5. General methods of different substitutions reactions at boron center of BODIPY dyes: (i) EtMgBr/Et_2O/3 h/22 °C; (ii) BCl_3/EtMgBr/Et_2O/ 3 h/ 22 °C; (iii) Et_2AlCl/CH_2Cl_2/25 °C/5 min; (iv) Ph-C≡C-Li or Ph-C≡C-H/EtMgBr

3 h (Scheme 5a). But the reaction becomes more facile with the use of Lewis acid reagents. For example, in combination with the BCl_3 and EtMgBr, the yield of the BEt_2-BODIPY increased to 98% (Scheme 5a) (Lundrigan et al. 2012). Further, with the use of Lewis acid Et_2AlCl, the reaction completes within 5 min to give high yield (78%) of the desired product, BEt_2-BODIPY (Scheme 5a) (More et al. 2014).

13.4 Photophysical Properties

BODIPY dyes are known for their outstanding photophysical properties which can be tuned by the chemical modification of the dye core. High extinction coefficient (ε_{max}) and high quantum yield of fluorescence (Φ_{fl}) are the trademark of the BODIPY dyes. The naked BODIPY without any substitutions at the pyrrole rings, **1** (Scheme 1) shows absorption spectra with the longest absorption peak (λ_{abs}) at 503 nm for S0-S1 transition and very low fluorescence with λ_{em} at 521 nm (Table 13.1). Both the absorption and emission spectra shift bathochromically as the substitutions increase around the pyrrole ring of the BODIPY core. For example, PM546 and PM567 (Scheme 1) have λ_{abs} of 493 nm and 518 nm respectively and they show bright greenish yellow fluorescence with λ_{em} of 504 nm and 534 nm respectively (Table 13.1). Boron substitutions do not change the absorption and fluorescence spectral position due to the tetrahedral structure of the boron center. Styryl BODIPY dyes show highly bathochromic shift in absorption and fluorescence spectra, and the bathochromic shift increases with the number of attached styryl groups. For example, λ_{abs} of mono, bis, tri, tetra-styryl BODIPYs (**9–12)** (Scheme 4) show >100 nm bathochromic shift. Mono and bis-styryl BODIPYs (**9, 10**) show orange and red fluorescence whereas dyes **11** and **12** emit in the NIR region. Aza-BODIPYs also show red shifted absorbance and fluorescence. Tetraphenyl aza-BODIPY, **2** (Scheme 2) shows red fluorescence whereas both the absorbance and fluorescence of aza-BODIPY **3** (Scheme 2) are in the NIR region (Table 13.1). Absorbance and fluorescence properties of other BODIPYs are discussed later during the discussion about their applications.

13.5 Applications of BODIPY Dyes

13.5.1 Laser Dye

Apart from the high fluorescence quantum yields and high extinction coefficients of the BODIPY dyes, their low intersystem crossing (ISC) rate and low triplet excitation coefficients over the laser spectral region made them highly efficient laser dyes (Mula et al. 2008). Few BODIPY dyes are known to perform better in terms of lasing efficiency and photochemical stability as compared to

Table 13.1 Photophysical parameters of the BODIPY dyes

Dye	λ_{abs} (nm)	ε_{max} (M^{-1} cm^{-1})	λ_{em} (nm)	Φ_{fl}
1[a]	503	54,000	521	0.05
PM546[b]	493	79,000	504	0.99
PM567[c]	518	71,000	534	0.84
2[d]	643	76,900	673	0.22
3[d]	710	108,600	732	0.46
9[e]	572	58,900	585	0.92
10[e]	645	116,400	660	0.37
11[e]	665	96,900	682	0.35
12[e]	689	127,900	710	0.34

[a] Data reported in toluene (Zhang et al. 2012)
[b] Data reported in MeOH (Gupta et al. 2013)
[c] Data reported in EtOH (Mula et al. 2008)
[d] Data reported in ACN (Wagner and Lindsey 1996)
[e] Data reported in $CHCl_3$ (Buyukcakir et al. 2009)

widely used Rhodamine 6G (Rh6G). Boyer and Pavlopoulos are the pioneers in exploring the lasing properties of the BODIPY dyes. Later on, during the late 1980s and early 1990s, Boyer and co-workers did extensive work to establish BODIPY dyes as highly efficient laser dyes in green yellow to the red spectral region (Shah et al. 1990; Boyer et al. 1993). Various BODIPY analogues were synthesized by changing the substituents at C-2, 6 and 8 (*meso*) positions of the dipyrromethene core (Fig. 13.2). Among these, pyrromethene 567 (PM567, 1,3,5,7,8-pentamethyl-2,6-diethylpyrromethene-difluoroborate complex), pyrromethene 546 (PM546, 1,3,5,7,8-pentamethylpyrromethene-difluoroborate complex), pyrromethene 597 (PM597, 1,3,5,7,8-pentamethyl-2,6-di-t-butylpyrromethene-difluoroborate complex) and pyrromethene 556 (PM556, disodium-1,3,5,7,8-pentamethylpyrromethene-2.6-disulfonate-difluoroborate complex) are highly efficient and most popular laser dyes in the green yellow region which are commercially available (https://www.photonicsolutions.co.uk). Among these dyes, PM567, PM546 and PM597 are used in organic solvents (mostly in ethanol), but PM556 is water soluble, thus useful in water based laser systems.

Despite very good optical properties, there are two major drawbacks of the BODIPY dyes such as their small Stokes shifts and low photochemical stability. The low Stokes shifts effectively enhances ground state absorption (GSA) which eventually decreases their lasing efficiency. On the other hand, faster phtodegradation reduces the laser operation life which is a big hurdle for the long-term operation of BODIPY liquid dye lasers. This becomes more severe problem in case of high average power and high repetition rate dye lasers (Mula et al. 2008).

It is suggested that the excited triplet state of the BODIPY dyes produced on photoexcitation transfers the energy to surrounding triplet oxygen ($^3O_2$) to generate singlet oxygen ($^1O_2$) which reacts at the C-8 olefin moiety of the dyes, leading to

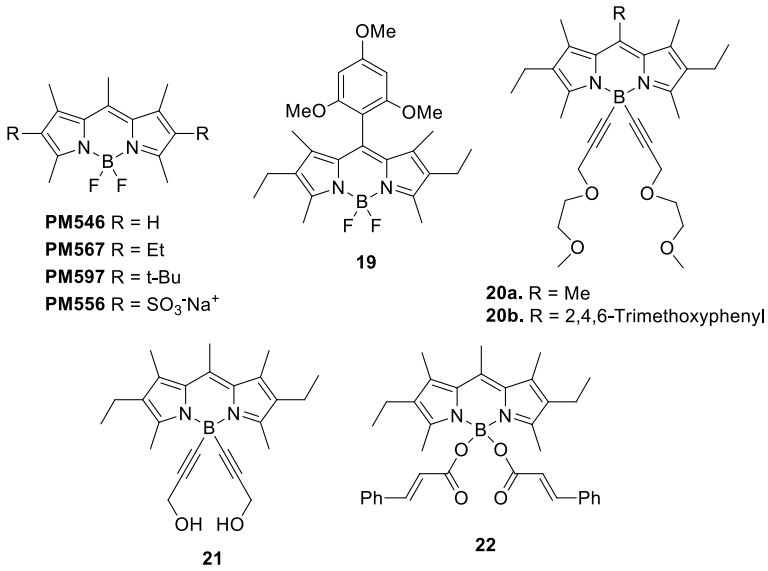

Fig. 13.2 Chemical structures of BODIPY laser dyes

their degradation (Mula et al. 2008). The entire $^1O_2$ generation process and photochemical decomposition of BODIPY dyes is schematically depicted in Fig. 13.3. The dye decomposition can be prevented by using a triplet quencher like benzoquinone (BQ) as well as trace amounts (1 wt% doping level) of antioxidants, such as DABCO, Tin770 and TBP, which supports the proposed dye degradation mechanism. Especially, the highest efficacy of the singlet oxygen-quencher, DABCO, amongst the additives strongly suggests $^1O_2$ as the major causative agent for the dye decomposition (Ray et al. 2007).

BODIPY dyes dispersed in solid matrix such as glass/polymer were also developed to enhance their laser output. In some of these matrices, BODIPY dyes showed better photostability as compared to liquid dye lasers. This is probably due to the unavailability of the oxygen in the solid matrix which reduces the chemical breakdown of the BODIPY dye structures.

Attempts were taken to improve photostability of the BODIPY dyes by their structural modifications. One such effort showed that substitution at the *meso* position of pyrromethene 567 (PM567) laser dye by aryl group increased the photostability (Mula et al. 2008). Especially, *meso*-trimethoxyphenyl BODIPY (**19**) (Fig. 13.2) was twofold more photostable with similar lasing efficiency as compared to PM567 at a significantly lower concentration. The dye **19** generates less $^1O_2$ due to low reactivity of the triplet dye with triplet oxygen. Also due to more steric crowding at *meso*-position, its reaction probability with the $^1O_2$ is lower as compared to PM567. All these enhance its photostability.

In other reports, boron substitutions were shown to enhance the photostability of the BODIPY dyes. For example, dye **20a** and **20b** (Fig. 13.2) with 2,5-dioxaoct-7-yne

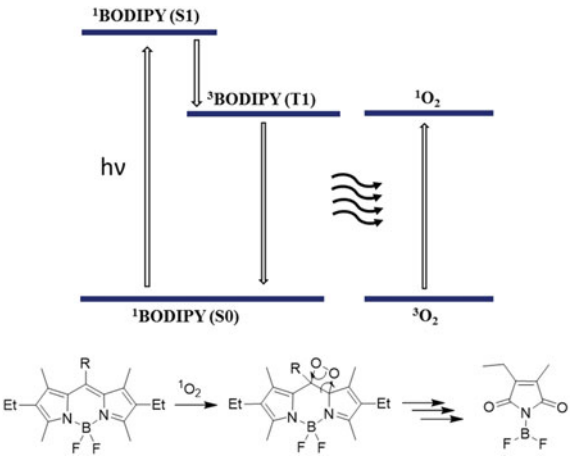

Fig. 13.3 Mechanism of singlet oxygen generation and photochemical decomposition of the BODIPY dyes

substitutions at the boron center of PM567 and BODIPY **19** respectively, were of high lasing efficient with higher photostability as compared to their precursors (Jagtap et al. 2013). Detailed theoretical calculations and pulse radiolysis investigation established that due to the boron substitutions, $^1O_2$ generation capacity of these dyes and also their rate of reaction with $^1O_2$ reduced which effectively increased their lasing life time. Further, the effect of solvent polarity change in the lasing efficiency and photostability of BODIPY dyes were investigated. The BODIPY dye **21** (Fig. 13.2) with propargyl alcohol substitutions at the B-center showed high lasing efficiency with higher photochemical stability as compared to PM567 in both polar (ethanol) and non-polar (1,4-dioxane) solvents (Gupta et al. 2017). The photostability of the dye **21** in 1,4-dioxane is comparable to that of Rhodamine 6G in ethanol, considered to be the benchmark for lasing photostability. The high photostability of dye **21** in the non-polar solvent 1,4-dioxane is mainly due to its low reactivity with $^1O_2$ which was confirmed by methylene blue-induced photo-degradation results, and this was further rationalized by theoretical calculations. Thus, combination of the substitutions at the B-center and use of non-polar solvents as lasing medium are useful to enhance the photostability of the BODIPY dyes immensely keeping their lasing properties unaffected.

Ray et al. developed series of COO-BODIPY laser dyes with outstanding lasing efficiencies and photostabilities (Ray et al. 2020). For example, dye **22** (Fig. 13.2) showed ~68% lasing efficiency as compared to 48% lasing efficiency of the well-known commercial laser dye, PM567 pumped under identical experimental conditions. The dye is highly photostable, no decrease in lasing efficiency was observed until 100,000 pumping pulses whereas 80% drop in lasing emission was found in case of PM567 under the same pumping period and experimental conditions.

BODIPY PM650 (Fig. 13.4), a methylated BODIPY dye with the *meso*-cyano group is a commercially available well known red-emitting BODIPY laser dye (λ_{peak} = 656.5 nm) (Belmonte-Vázquez et al. 2019). The electron withdrawing *meso*-cyano

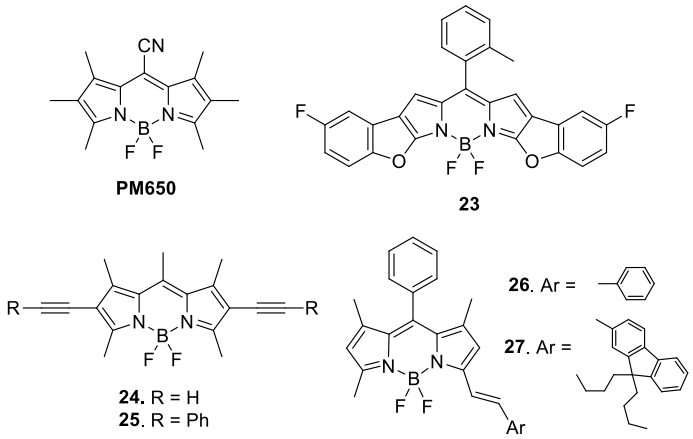

Fig. 13.4 Chemical structures of red shifted BODIPY laser dyes

group lowers its reactivity with the singlet oxygen, responsible for the photodegradation mechanism which eventually makes it highly photostable (tolerance of ≤6.3 GJ/mol). Belmonte-Vázquez et al. synthesized a family of benzofuran-fused BODIPY dyes with bright fluorescence and high lasing efficiencies (>40%) toward the red edge of the visible spectrum (Belmonte-Vázquez et al. 2019). Among these dye **23** has better (43%) lasing efficiency as compared to PM650 (31%) in similar conditions, and its photostability (tolerance of ≤7.4 GJ/mol) surpasses that of the reference dye PM650.

Using the metal mediated cross-coupling reaction discussed *vide supra*, extended π-conjugated dyes, 2,6-diacetylenyl and 2,6-bis(phenylacetylenyl)-BODIPY derivatives (**24** and **25**) were synthesized for lasing applications in the red spectral region (Fig. 13.4) (Maity et al. 2017). Dye **24** and **25** showed stable lasing efficiencies of 41% (tuning range: 561–580 nm) and 36% (tuning range: 602–617 nm) respectively under continuous transverse pumping at 532 nm for 180 and 110 min respectively.

Zhang et al. synthesized a series of highly fluorescent red shifted BODIPY dyes by increasing π-conjugation length as well as tuning Intramolecular Charge Transfer (ICT) effect (Zhang et al. 2011). These dyes showed stable laser emission with high efficiencies in the green to near IR spectra region (570–725 nm) (Zhang et al. 2011). Among these dyes, dye **26** and **27** (Fig. 13.4) showed 46% (λ_{lasing}: 559 nm, pumped at 532 nm) and 57% (λ_{lasing}: 596 nm, pumped at 570 nm) lasing efficiencies respectively.

Thus, tremendous molecular engineering was done to synthesize functional BODIPY laser dyes applicable in the UV–Vis to NIR region. Different strategies were also adopted to enhance their photostability to increase lasing life time.

13.5.2 Chemical and Bio-sensors

Fluorescence based sensors are highly popular due to their high sensitivity, selectivity, rapid response, simplicity, low sample requirements, non-destructiveness etc. Organic dye based chemo- and bio-sensors are mostly relying on modulation of their fluorescence properties upon trapping the analyte. These kinds of efficient chemo- and bio-sensors are very useful in analytical chemistry as well as in clinical, medical, and environmental applications. Fluorescence changes in these sensors occur mainly *via* Photoinduced Electron Transfer (PET) or by Photoinduced Charge Transfer (PCT) or by the Fluorescence Resonance Energy Transfer (FRET) mechanism. Thus, the key design of these molecules includes chemical attachment of some pre-designed site capable of trapping the analytes which changes the fluorescence of the sensor. In this manner, recognition of the analyte can enhance (turn-on) or decrease (turn-off) the fluorescence, but in conventional design, turn-on fluorescence of the sensor in the presence of an analyte is preferred. Change in fluorescence colour of the sensor (ratiometric sensing) after trapping the analyte is also very interesting. Potential of the BODIPY dyes as the molecular sensor was first explored by Daub and Rurack and after that numerous examples of BODIPY-based fluorescent chemo- and bio-sensors were reported (Boens et al. 2012).

BODIPY dyes containing *p*-(N,N-dialkyl)aniline subunit were used extensively as pH sensors. These dyes are low/non-fluorescent due to PET from anilino group to BODIPY core which can be prevented by protonation of the anilino moiety and thus the dyes become fluorescent after protonation due to prevention of PET. For example, *meso p*-(N,N-dialkyl)aniline substituted BODIPY **28** (Fig. 13.5) acts as highly efficient "turn-on" type pH sensor in the greenish-yellow spectral region (Boens et al. 2012). Subsequently, red shifted 3,5-distyryl-BODIPY dye (**29**) (Fig. 13.5) were synthesized via Knoevenagel type condensation reactions discussed vide supra. Dye **29** was low fluorescent ($\lambda_{abs} = 700$ nm, $\lambda_{em} = 753$ nm, $\Phi_{fl} = 0.18$) in the neutral state but in the presence of acid, both the absorption and emission bands hypsochromically shifted and it lit up ($\lambda_{abs} = 620$ nm, $\lambda_{em} = 630$ nm, $\Phi_{fl} = 0.68$) (Ziessel et al. 2009). It was covalently attached with the porous polyacrylate beads and efficiently used as the solid-state colorimetric and fluorescent sensor for analysis of HCl in a gas stream and aqueous solution.

Ratiometric pH sensor based on BODIPY dyes are also known. Imino-BODIPY dye **30** (Fig. 13.5) showed dramatic colour change from pink to yellow in the presence of acid due to the cleavage of its acid-labile imine group. This also resulted in change in fluorescence from orange to green in the pH range of 1.8 to 7.4 (Gupta et al. 2013).

Several anilino substituted BODIPY dyes were also exploited for detection and quantification of various metal ions as well as other important analytes. For example, *meso*-ortho phenylenediamine BODIPY (**31**) is non-fluorescent due to photo-induced electron transfers of amino lone pairs to the BODIPY core. But both the amine residues are highly reactive towards nitric oxide (NO) to form dye **32** which is highly fluorescent (Fig. 13.6). This fluorescence enhancement of dye **31** in the presence of NO was used for efficient detection of in situ generated NO (Gabe et al. 2004). Nitric

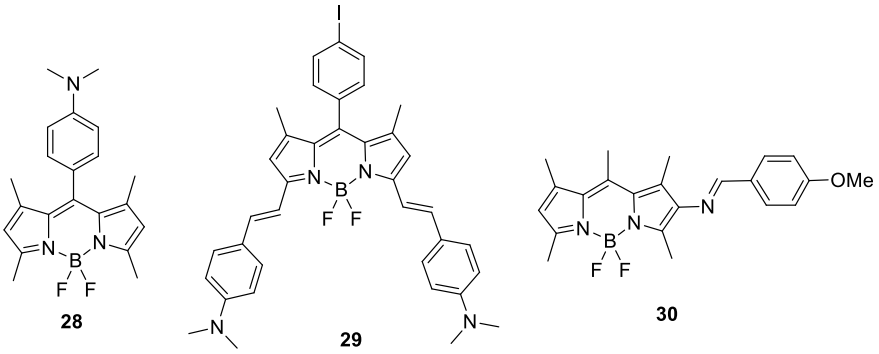

Fig. 13.5 BODIPY based pH sensors

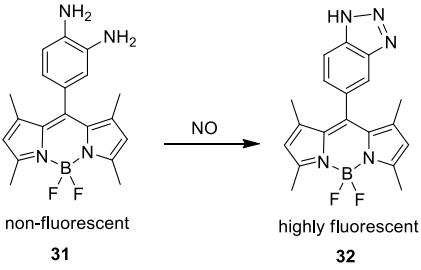

Fig. 13.6 Reaction of *meso*-ortho phenylenediamine BODIPY (**31**) with NO

oxide imaging in living cells using other BODIPY dyes is also discussed *vide infra* in the cellular imaging section.

Adopting the similar strategy, anilino-BODIPY dyes with coordinating ligands were used as sensor for different alkali and transition metal ions. For example, BODIPY dye **33** (Fig. 13.7) with the 13-phenyl-1,4,7,10-tetraoxa-13-azacyclopentadecane chelator is non-fluorescent, but after complexing with different alkali (Li^+, Na^+) and alkaline-earth (Mg^{2+}, Ca^{2+}, Sr^{2+}, Ba^{2+}) metal ions, it became highly fluorescent showing its capability as the metal sensor (Kollmannsberger et al. 1998). The metal specificity was tuned with a different chelator. BODIPY dye **34** (Fig. 13.7) with the *meso*-16-phenyl-1,4,7,10,13-pentaoxa-16-azacyclooctadecane chelating group binds efficiently with Pb^{2+} ion showing turn-on fluorescence (Mbatia et al. 2010). Chang et al. used a mixed N/O/S receptor based ligand to synthesize water soluble BODIPY dye **35** (Fig. 13.7) which showed highly selective turn-on fluorescence in the presence of Ni^{2+}. Dye **35** is capable of detecting intracellular Ni^{2+} and did not show any fluorescence response with the other biologically abundant metal ions (Dodani et al. 2009).

Different other strategies were also used to develop BODIPY based metal sensors. BODIPY-phenanthroline conjugate **36** ($\lambda_{em} = 535$ nm) and BODIPY-acetylacetone conjugate **37** ($\lambda_{em} = 570.0$ nm) (Fig. 13.7) were shown to have selective Cu^{2+} sensing ability where both the dyes showed turn-off fluorescence responses due

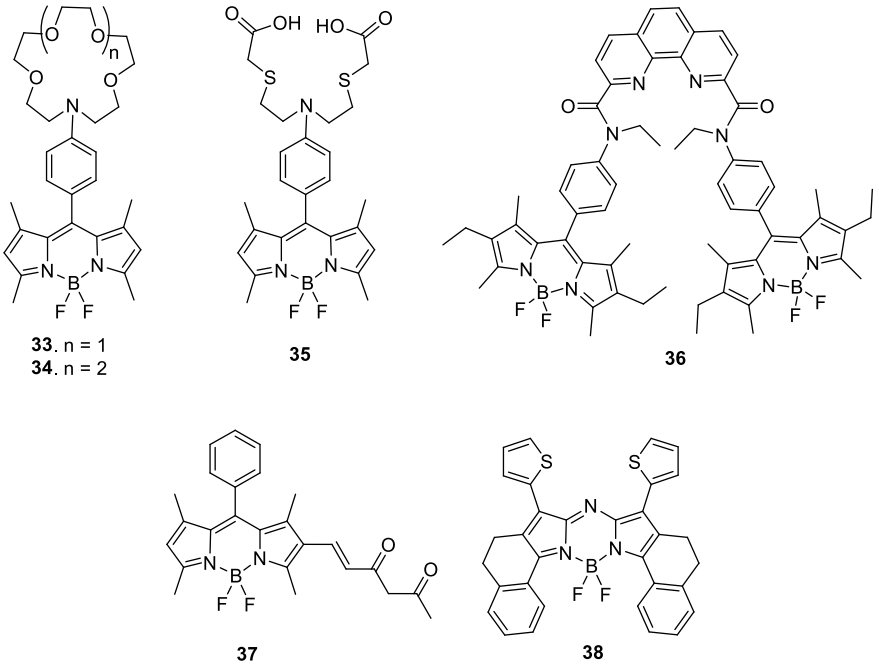

Fig. 13.7 Metal sensitive BODIPY dyes

to BODIPY to metal charge transfers (More et al. 2017; Gorai et al. 2022). Xiao et al. developed a highly selective near-infrared fluorescent probe for Hg^{2+} based on thiophene containing aza-BODIPY **38** ($\lambda_{em} = 782$ nm) (Fig. 13.7) (Jiang et al. 2016). Hg^{2+} ion coordinated with the C-8 N and S atoms of 1,7-thienyl groups inhibiting the free rotations of the thienyl groups. This caused intramolecular charge transfer from thienyl groups to the aza-BODIPY moiety leading to fluorescence quenching. The probe was also shown to detect Hg^{2+} in living cells. Zn^{2+} ion sensing using BODIPY dye and its application is discussed *vide infra* in the cellular imaging section.

BODIPY based efficient bio-sensors are also well-known. BODIPY based fluorescence techniques were developed for detection and quantification of proteins useful for clinical applications. Chang et al. synthesized a mega Stokes shift BODIPY-triazole dye (**39**) (Fig. 13.8) capable of very specific binding with human serum albumin (HSA) as compared to other serum albumins showing 220-fold fluorescence enhancement. Successful quantification of HSA in urine samples within the concentration limits of micro-albuminuria using dye **39** showed its potential in clinical application ability (Er et al. 2013).

BODIPY dyes are also extensively used for the detection of protein fibrils which are highly important for the diagnosis and treatment of amyloid related neurological diseases. Detection of self-assembly of diphenylalanine into nanofibers is very important to get the mechanistic inside of the β-amyloid aggregation which is the central cause for the Alzheimer's disease. Quan et al. reported that the green BODIPY dye

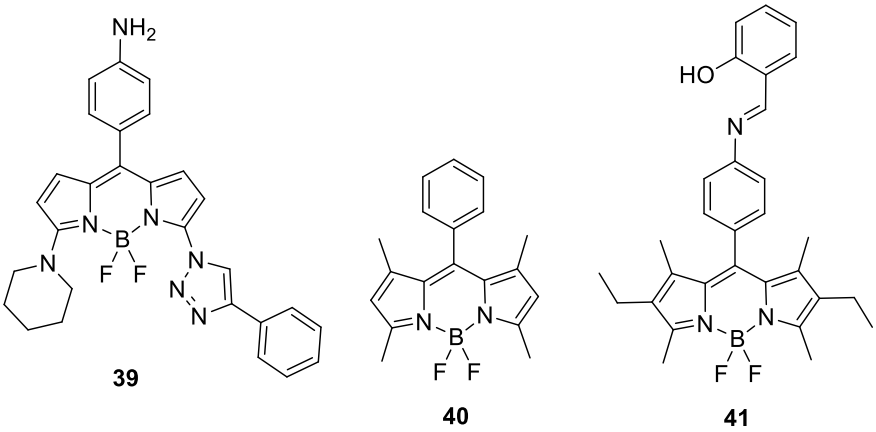

Fig. 13.8 BODIPY dyes used for detection of protein and protein fibrils

40 (Fig. 13.8) showed very high turn-on fluorescence with nanofibers of diphenylalanine, thus can be useful for early detection as well as drug development of Alzheimer's disease (Quan et al. 2019).

Nath et al. also developed a turn-on fluorescent based NIR-emitting BODIPY glycoside probe for detection of matured insulin fibrils (Mora et al. 2021). Most importantly the probe can also detect oligomers formation from the native protein. The probe can be useful for the in vivo imaging of protein oligomers and matured fibrils. In a separate report they also investigated the structure activity relationship of a BODIPY-salicylaldimine Schiff base (**41**) (Fig. 13.8) and its corresponding boron complex dye for their sensitivity towards amyloid fibrils from hen-egg white lysozyme (Sen et al. 2022). The dye **41** showed high fluorescence enhancement as compared to its boron complex upon binding with lysozyme fibrils.

13.5.3 Cellular Imaging

Outstanding fluorescence properties along with the easy cell permeability of the BODIPY dyes (due to its hydrophobicity) made them highly useful candidates for developing cellular imaging agents. Due to their relatively high lipophilicity, they tend to accumulate in the subcellular membranes. Additionally, several molecular engineering techniques were done to develop organelle specific imaging agents.

For example, BODIPY dye **42** (Fig. 13.9) showed preferential localization in the endoplasmic reticulum (ER) confirmed by co-staining experiments (Jiao et al. 2010). The commercially available ER-Tracker™ Red (BODIPY™ TR Glibenclamide) is a highly selective ER staining dye. In this, green-fluorescent BODIPY™ TR dye is attached with glibenclamide which is very specific to bind with the sulphonylurea receptors of ATP-sensitive K^+ channels present in ER.

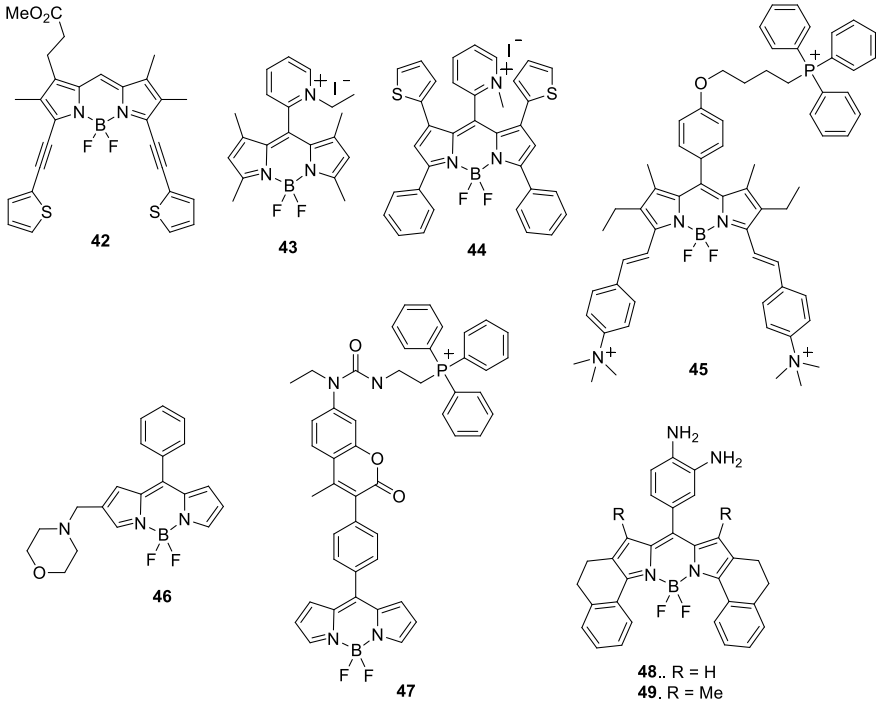

Fig. 13.9 BODIPY dyes for cellular imaging

Several mitochondria specific BODIPY dyes were also developed. As mitochondria is negatively charged, the positively charged dyes tend to accumulate in it. In general, BODIPY dyes are neutral, thus cationic moieties such as ammonium, pyridinium, phosphonium moieties were chemically inserted in the BODIPY core to synthesize positively charged BODIPY dyes for mitochondria imaging. For example, the pyridinium BODIPY dyes **43** (Zhang et al. 2013) and **44** (Jiang et al. 2013) (Fig. 13.9) are water soluble and photostable mitochondria targeting dyes useful for imaging. Jiang et al. developed a red emitting distyryl BODIPY dye (**45**) (Fig. 13.9) as an excellent alternative to the commercially available Mito Tracker Red (Wang et al. 2021). The ammonium groups increased its water solubility and the phosphonium group enhanced its mitochondria targeting ability. The dye penetrates the cellular and mitochondrial membranes and accumulates in mitochondria in high densities. Additionally, it showed low photobleaching and phototoxicity as compared to Mito Tracker Red which established it as an excellent mitochondria imaging dye.

Several BODIPY based viscosity probes were developed to visualize intracellular viscosity changes. Molecular rotor based BODIPY dyes are used for this purpose as these dyes showed restricted bond rotation in viscous medium which changed their fluorescence properties. For example, dye **46** (Fig. 13.9) was synthesized to probe lysosomal viscosity changes (Wang et al. 2013). The attached morpholine moiety

made it lysosome specific dye and, reduction in PET from morpholine to BODIPY core in lysosomal acidic environment as well as viscosity driven restricted rotation of the *meso*-phenyl group turn-on its fluorescence.

The dye **47** (Fig. 13.9) was developed for the mitochondrial viscosity measurement. The dye was designed in such a way that the attached phosphonium moiety made it mitochondria targeting and the *meso*-coumarinylphenyl formed molecular rotor structure which showed viscosity responsive turn-on fluorescence of BODIPY core at 516 nm (Yang et al. 2013). The coumarin fluorescence (427 nm) remained unchanged with viscosity change, thus the intensity ratio of BODIPY to coumarin emission peaks showed linear response with increase in viscosity. Using this dye mitochondrial viscosity in living HeLa cells was determined as 62 cP which increased to 110 cP upon treatment with an ionophore like monensin or nystatin.

Nitric oxide (NO), an endogenously produced gaseous signaling molecule can be visualized in cells by using a highly reactive dye. Reactivity towards NO and fluorescence turn-on behaviour of o-phenylenediamine-BODIPY moiety was discussed *vide supra*. A similar strategy was adopted for imaging of NO in cells and tissues. The NIR-fluorescent BODIPYs **48** and **49** (Fig. 13.9) were highly sensitive NO probes showing >400-fold increase in fluorescence intensity in the presence of NO with very low detection limit i.e. 2.1 nM and 0.6 nM respectively. Both the dyes were cell-permeable and capable of NO imaging in living cells without any cytotoxicity (Zhang et al. 2014).

13.5.4 Photodynamic Therapy

Cancer is the leading cause of death, accounting for millions of deaths every year worldwide. Thus, research and treatment of cancer is an urgent topic where almost all the developed countries are spending huge amount of money every year. Most popular tumor therapies are surgery, chemotherapy and radiotherapy. Compared to these, photodynamic therapy (PDT) is relatively a new treatment modality for malignant tumors which has many unique advantages such as (a) useful for the site/organ unsuitable for surgery; (b) suitable for people (infirm, the elderly etc.) not fit for surgery, chemotherapy and radiotherapy; (c) safe and effective reusability; (d) does not suppress the immune system; (5) useable after or at the same time in a synergistic way with surgery, chemotherapy and radiotherapy (Brown et al. 2004).

Photodynamic therapeutic agents are the triplet photosensitizers (PSs) in which intersystem crossing (ISC) is very efficient. Thus, triplet photosensitizers absorb light to excite to their singlet excited state and then eventually go to the triplet state via efficient ISC. Then the radiative decay of the triplet state i.e. phosphorescence occurs which has a long lifetime (microseconds and above). This radiative energy excites the ground sate oxygen (triplet oxygen) to generate singlet oxygen ($^1O_2$) (Fig. 13.3) which is highly reactive and subsequently generates different reactive oxygen species (ROS). ROS including $^1O_2$ are responsible for the killing of the cancer cells where the triplet photosensitizers are accumulated.

Currently, porphyrin derivatives, such as porfimer sodium (Photofrin), protoporphyrin IX, and temoporfin etc. are the most studied photosensitizers for PDT applications (Ethirajan et al. 2011). Although they have their own shortcomings such as, small Stoke shift, low molar absorptivity ($<2 \times 10^4$ cm^{-1} M^{-1} in the range of 650–900 nm), high aggregation tendency due to strong π-π stacking which can reduce the quantum yield of $^1O_2$, synthetic inaccessibility which restricts the production in large amount by conventional organic synthetic strategy etc. Other non-porphyrin photosensitizers such as phthalocyanine, squarine dye and perylene diimide were reported for PDT study, however poor chemical and photostability and, aggregation in a polar environment restrict their practical applications (Wainwright 1996).

In the past decade, BODIPY class of dyes have been established as a promising PDT agent due to their exceptional photophysical properties (Kamkaew et al. 2013; Turksoy et al. 2019). The intersystem crossing (ISC) can be facilitated by the attachment of heavy atoms which eventually increases singlet oxygen yield. Therefore, it is a widely adopted strategy for the development of efficient PDT molecules. Thus, similar strategy was also used to design BODIPY based PDT molecules. Chemically, all the positions of the BODIPY core are reactive for heavy atom (Br/I) addition without disrupting the planarity of the dye. Additionally, cellular localization of these photosensitizers also can be ascertained by the fluorescent imaging technique.

O'shea et al. synthesized 2,6-dibromo aza-BODIPY chromophore (**50**, **51**) which showed efficient singlet oxygen generation at lower concentrations as compared to their parent BODIPY dyes (Fig. 13.10) (Killoran et al. 2002; Gorman et al. 2004). Yogo et al. synthesized the simple 2,6-diiodo BODIPY dye **52** (Fig. 13.10) which showed 1.34 times greater $^1O_2$ generation as compared to well-known PDT photosensitizer Rose Bengal (Yogo et al. 2005).

Further, different iodo-substituted BODIPY dyes were synthesized to check the effects of halogen substitution patterns on the photosensitizing ability of BODIPY dyes which eventually helped to increase the heavy atom effect (Ortiz et al. 2012). The study showed that the substitution of iodine at 2 and 6 positions has the highest impact on singlet oxygen generation (**53**, **54**). Iodine substitution at 3,5-positions (**55**, **56**) did not show any distinct increase in singlet oxygen generation efficiencies (Fig. 13.10).

Thus, 3,5-positions of BODIPY core were used to extend π-conjugation for the synthesis of near-infrared (NIR) absorbing dyes useful for practical application in the body's therapeutic window (650–900 nm). Further, other functionalities were also added to induce water solubility, cancer cell affinity etc. For example, Atilgan et al. developed 2,6-dibromo/iodo-3,5-distyryl derivatives with or without polyethylene glycol (PEG) side chains (**57**–**59**) (Fig. 13.10) (Atilgan et al. 2006). The halogens were used to generate $^1O_2$, styryl units extended conjugation to the NIR region (650–680 nm) and water-soluble PEG groups enhance their solubility in aqueous solutions, cell permeability and tumor targeting properties. Beside all these, PEG helps in alleviating aggregate formation in aqueous condition which is the main reason for inefficient formation and potential quenching of the triplet state of the dye and singlet oxygen. Compound **59** ($IC_{50} = 11$ $ngmL^{-1}$) was the most potent candidate showing even higher photocytotoxicity as compared to the most used photosensitizer

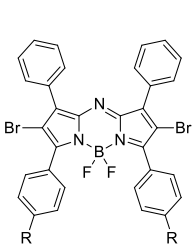

50. R = H
51. R = OMe

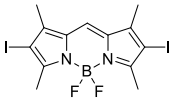

52

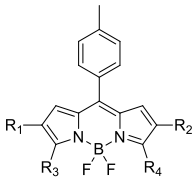

53. R_1 = I; $R_2 = R_3 = R_4$ = H
54. $R_1 = R_2$ = I; $R_3 = R_4$ = H
55. $R_1 = R_2 = R_3$ = I; R_4 = H
56. $R_1 = R_2 = R_3 = R_4$ = I

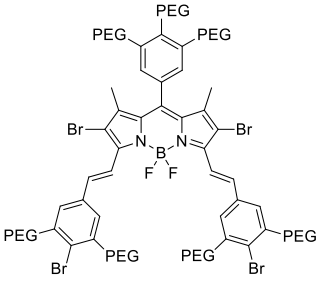

PEG = $O(CH_2CH_2O)_3CH_3$

57

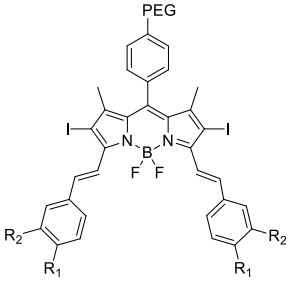

58. $R_1 = OCH_3$; R_2 = H
59. $R_1 = R_2 = O(CH_2CH_2O)_3CH_3$

Fig. 13.10 Halogenated BODIPY dyes for PDT applications

porfimer sodium ($IC_{50} = 4600$ ngmL^{-1}) under the same condition. This is probably due to its low aggregation and high cellular uptake in the biological environment due to attached triethylene glycol chains.

It is well established that the attachment of heavy atoms enhances dark toxicity, decreases triplet state lifetime and, changes bio-distribution and pharmacokinetics of the PDT agents. Thus, heavy-atom-free organic triplet photosensitizers (PSs) are advantages for practical applications. Several heavy atom free BODIPY dyes are also reported to be used as PDT photosensitizers. Shivran et al. synthesed water-soluble BODIPY glycosides with different fluorescence colour and studied their efficiencies as PDT agents (Shivran et al. 2016). Amongst them glycosylated mono-styryl-BODIPY dye **60** ($\lambda_{abs} = 573.8$ nm and $\lambda_{em} = 590$ nm) (Fig. 13.11) showed best PDT activities against the A549 cell line and importantly it is non-toxic to normal lung cells.

Orthogonal BODIPY dimers (Bis-BODIPYs) are another class of heavy atom free BODIPY dyes for potential singlet oxygen photosensitization (Cakmak et al. 2011). As compared to their monomer ($\lambda_{abs} = 530$ nm), the dimer **61** (Fig. 13.11) showed split band absorption maxima (490 and 560 nm) and large Stokes shift (>80 nm) with decreased florescence quantum yield. High ISC from singlet to triplet excited state resulted in high quantum yield of singlet oxygen production (0.4 in toluene and 0.5

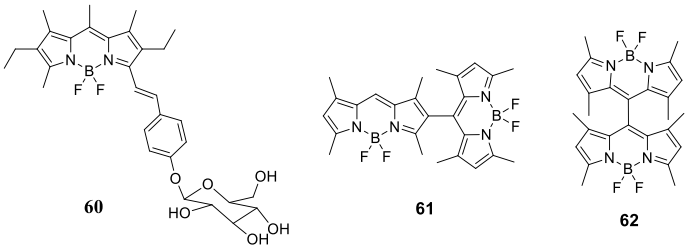

Fig. 13.11 Heavy atom free BODIPY dyes for PDT applications

in dichloromethane) whereas the monomer produces very low $^1O_2$ (<0.1). On the other hand, dimers **62** (Fig. 13.11) showed lower singlet oxygen quantum yield with significant florescence emission and thus promising for dual use as therapeutic and imaging agents.

Thus, both halogenated non-halogenated BODIPY PDT agents were developed. Some of the dyes showed high photosensitizing ability. Further experimentations are required to establish them as clinically applicable PDT agents.

13.5.5 Fluorescent-Positron Emission Tomography Probes

High resolution molecular imaging techniques are important for diagnostic and therapeutic purpose i.e., in vivo imaging of specific biological pathways at the molecular and cellular level. Various high-end imaging techniques are available such as Computed Tomography (CT), Single Photon Emission Computed Tomography (SPECT), Positron Emission Tomography (PET), bioluminescence, fluorescence and Magnetic Resonance Imaging (MRI) etc. But all these molecular imaging techniques have their own advantages and limitations in spatial and temporal resolution, depth penetration, sensitivity and cost (Tsien 2003). Thus, fusion of two or more techniques can be very useful to obtain synergistic effect avoiding these limitations of each individual techniques. PET-CT, PET-MRI are the examples of such dual imaging techniques. Similarly, PET-fluorescence dual modality imaging technique could be of highly beneficial for clinical applications. PET is a sophisticated imaging technique useful for noninvasive diagnosis of cancer via locating the in vivo distribution of radio labeled biomolecules. In contrast, fluorescence imaging is a superior technique useful for intra operative tumor detection (Nguyen et al. 2010). Thus, due to these complementary natures of PET and optical imaging techniques, PET/fluorescence dual modality imaging technique might be greatly useful for both diagnosis and therapeutic purpose of cancers. Noninvasive PET scans will be useful for locating the lesion (diagnosis), and intra operative fluorescence image-guided surgery will be helpful for the surgeons to identify the PET-detected lesions or smaller metastasis (therapy).

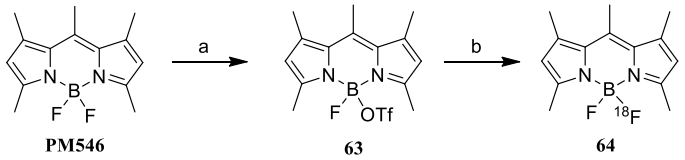

Scheme 6. Synthesis of ^{18}F-BODIPY dye: (a) TMSOTf, 20 °C, 1 min; (b) $^{18}F^{-}$, 20 °C, 1 min

BODIPY dyes are advantageous over other well-known fluorescent dyes for intracellular imaging within living cells as discussed vide supra. Due to their neutral nature, they efficiently penetrate the cell membranes Additionally, ^{19}F/^{18}F exchange is possible at the BF_2 group present in the central core to develop hybrid ^{18}F PET/optical imaging agents.

Few methods are reported to synthesize ^{18}F-BODIPY, among them the easiest method was described by Mazitschek et al. First, activated BODIPY triflate (**63**) was synthesized (1 min, near quantitative yields) followed by addition of free $^{18}F^{-}$ which converts it to ^{18}F-BODIPY (**64**) almost instantly (Scheme 6) (Hendricks et al. 2012). The method is easily reversible, rapid, and efficient in incorporation of 18-fluoride in the BODIPY core.

Hyunjung Kim et al. synthesized a red shifted ^{18}F-BODIPY dye **65** ($\lambda_{abs} = 580$ nm and $\lambda_{em} = 590$ nm) (Fig. 13.12) useful for PET/fluorescence imaging of brain (Kim et al. 2019). PET/optical imaging data showed that it was suitable for brain penetration with desirable brain pharmacokinetics of the radio ligand and thus can be widely used as a prosthetic group for the brain hybrid PET/optical imaging agent. Further ^{18}F-BODIPY dye (**66**) (Fig. 13.12) was developed by Giuseppe Carlucci et al. for dual-modality optical/PET imaging of PARP1 in Glioblastoma (Carlucci et al. 2015). The fluorescent component of **66** enables optical imaging with cellular resolution, while the radiolabeled component helps whole-body deep-tissue imaging of malignant growth. Thus, BODIPY dyes showed high promise as fluorescent-PET probes for the development of PET/fluorescence dual modality imaging technique.

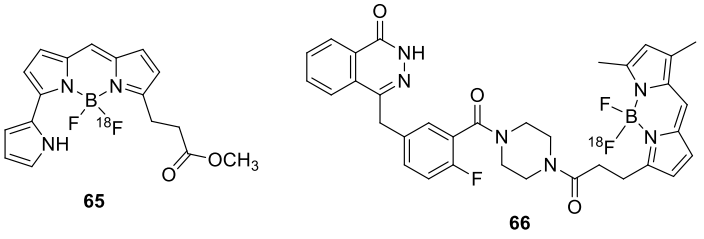

Fig. 13.12 ^{18}F-BODIPY dyes for PET/optical dual imaging

13.5.6 Organic Photovoltaics (OPV)

Development of organic small molecules for efficient solar energy conversion into chemical energy is a major contemporary challenge for chemists. In the photosynthesis processes, natural photosynthetic organisms act as efficient antennas to absorb photons in the visible spectrum and then funnel energy to the reaction center for photosynthesis. Mimicking this, several BODIPY based light-harvesting systems were developed. High extinction coefficient, wavelength tuning from UV–Vis to NIR regions, good electron mobility etc. are the positive elements which made BODIPY to be considered for futuristic organic photovoltaics.

Ziessel et al. first developed synthetic strategies for polyaromatic appended BODIPY dyes with the aim that the energies absorb by the ancillary light absorbers will channel to the BODIPY core. In this way, several dual-dye systems (**67**–**70**) (Fig. 13.13) were synthesized and efficient energy transfer (90%) were shown from the attached aromatic polycycles to the BODIPY core (Ulrich et al. 2008).

Further, this concept was extended to develop highly sophisticated energy transfer cassette **71** (Fig. 13.14) where dyads of pyrene and yellow fluorescent BODIPYs are connected with NIR fluorescent BODIPY dye via 1,4-phenylene-diethynylene moieties (Harriman et al. 2009). In **71**, excitation of the pyrene moiety at 370 nm resulted in bright red emission at 670 nm ($\Phi_{fl} = 51\%$) which confirms highly efficient energy transfer from blue fluorescent pyrene to green fluorescent BODIPY to ultimately red fluorescent BODIPY fluorophore. This type of light-harvesting system with wide absorption band are extremely useful for developing organic solar cells.

Leclerc et al. developed strategies to synthesize ethynylene and vinylene bridged dumbbell-shaped triazatruxene-BODIPY conjugates for bulk heterojunction (BHJ) solar cells (Bulut et al. 2017). Both the dyes were used as electron donor in devices formed in blending with phenyl-C71-butyric acid methyl ester ($PC_{71}BM$) as the electron acceptor. The ethylene bridged triazatruxene-BODIPY conjugate **72** (Fig. 13.15)

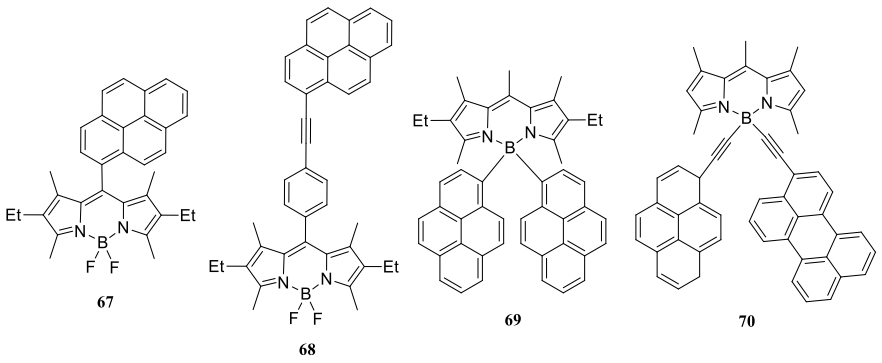

Fig. 13.13 BODIPY dyes attached with secondary polycycle chromophores as ancillary light absorber

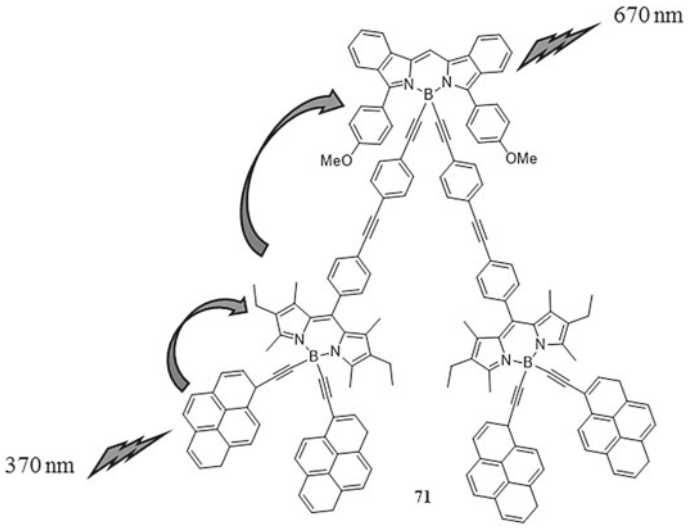

Fig. 13.14 Light-harvesting system containing different coloured BODIPYs and pyrenes

showed high power conversion efficiency of 5.8%. Singh et al. synthesized dithiafulvalene decorated BODIPY core (BODIPY-DTF, **73**) (Fig. 13.15) with efficient electron donor capacity. The OPV devices fabricated by blending BODIPY-DTF and $PC_{71}BM$ as electron acceptor showed highly efficient (7.2%) solar energy conversion (Srinivasa Rao et al. 2017). Several other BODIPY based small molecules showed excellent potential for being used as artificial light harvesters (Bessette and Hanan 2014).

13.5.7 Self-assembled Architectures

Soft materials and nanoparticles prepared from self-assembly of monomers show diversified property useful for numerous applications. Gels, dendrimers, liquid crystals, micelles, liposomes, microcapsules etc. are examples of different soft materials. These kinds of soft materials were also prepared by self-assembly of functional BODIPY based compounds for chemical, biological and optical applications. Ziessel et al. did the pioneering work in this area by incorporating the pre-designed BODIPY core into different supramolecular assemblies to develop coloured liquid crystals and organogels.

For example, 1:2 complex of yellow fluorescent anionic dye (**74**) and red fluorescent cationic dye (**75**) formed liquid crystals on heating in room temperature to above 150 °C (Fig. 13.16) (Olivier et al. 2012). Highly efficient energy transfer from the yellow fluorescent dye to the red fluorescent dye was observed in the mesomorphic state, thus it can be used as the light harvesting array on solar cell applications.

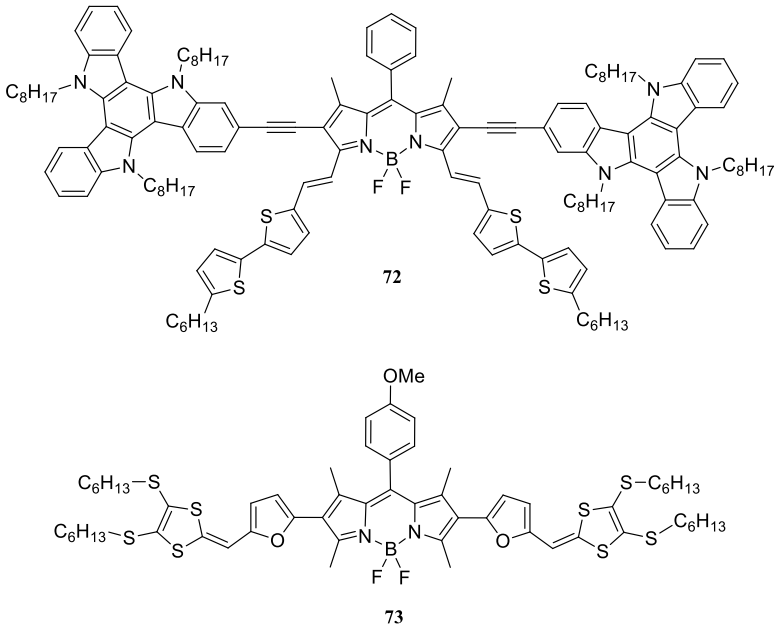

Fig. 13.15 BODIPY dyes for solar energy conversion

In another report, green and red emitting dyes were coupled with different generations of dendrimers to develop differently coloured liquid crystals (**76**–**79**) (Fig. 13.16) (Mula et al. 2015). The supramolecular assembly differs with the dendrimers generation, such as smectic A and C phases were observed with first-generation dendrimers whereas second- and third generation dendrimers showed nematic and/or smectic A phases.

Self-assembled BODIPY nanoparticles were shown to have great potential as sensors for important biological analytes. Amphiphilic BODIPY-*O*-glycoside dye **80** (Fig. 13.17) was reported to be self-assembled in aqueous solution to form non-fluorescent nanoparticles (NPs) (Shivran et al. 2021). These NPs showed high fluorescence enhancement in the presence of serum albumin, thus useful for selective detection and quantification of serum albumin. Human serum albumin (HSA) detection in urine samples were also shown using these NPs. In another report, self-assembled non-fluorescent nanoparticles (NPs) of BODIPY dye **81** (Fig. 13.17) showed selective turn-on fluorescence in the presence of Zn^{2+}. This was used in detection and quantification of Zn^{2+} in human hair (Jia et al. 2016).

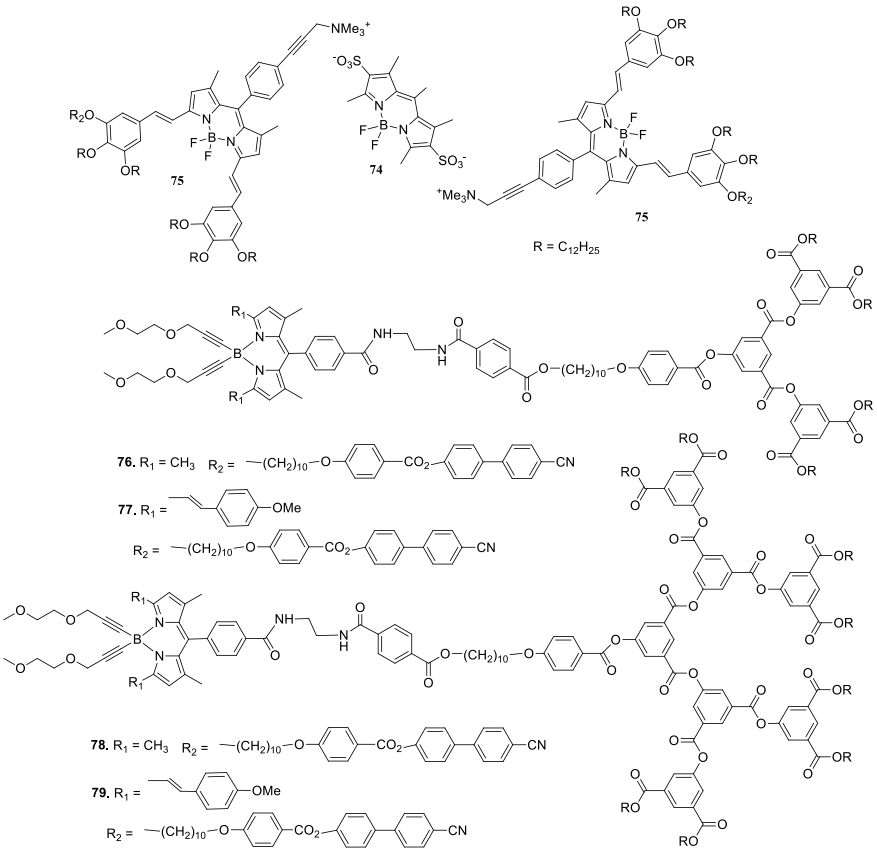

Fig. 13.16 Chemical structures of BODIPY based compounds showing liquid crystal properties

13.5.8 Photocatalysis

BODIPY dyes are also established as an efficient photocatalyst in various important organic reactions as well as chemical processes. Triplet state of the dye is responsible for the catalytic behaviour of the BODIPY dyes. During de-excitation of the triplet state, singlet oxygens are generated (Fig. 13.3) which are shown to be efficiently catalyzed organic reactions. For example, reaction of sulfides with singlet oxygen produce sulfoxides which are important intermediates for the total synthesis of biologically relevant molecules. BODIPYs are successfully used for photooxidation of sulfides into sulfoxides. BODIPY dye **40** was used to oxidize thioanisole (**82**) to corresponding methyl phenyl sulfoxide (**83**) quantitatively which took 24 h to complete the reaction. But the corresponding diiodo compound **84** took only 3 h to complete the reaction (Scheme 7) (Li et al. 2013). Dye **84** has higher ISC (triplet

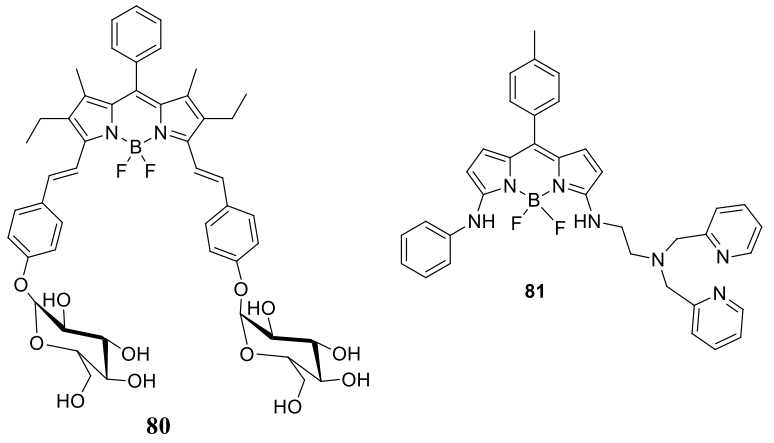

Fig. 13.17 Chemical structures of BODIPY dyes form self-assembled nanoparticles useful for sensing important biological analytes

quantum yield 0.83%) i.e. it generates higher $^1O_2$ generation as compared to **40** (triplet quantum yield 0.01%) which increases its photocatalytic activity.

BODIPY dye **84** is also very effective in photocatalytic oxidation naphthols to corresponding naphthoquinones. For example, dye **84** under visible light excitation (35 W Xe lamp) converts 1-naphthol to 1,4-naphthoquinone (**86**) in 1.5 h with 74% conversion yield (Huang et al. 2013). The 1,4-naphthoquinone was further reacted with substituted anilines and copper acetate to synthesize aminonaphthoquinones in a one pot reaction. The adduction product **87** was obtained in very good yield (75%) (Scheme 7). The yield of aminonaphthoquinone **87** was higher when BODIPY dye **84** was used as a photocatalyst as compared to well-known photocatalyst, tetraphenylporphyrin (TPP). The higher photocatalytic activity of **84** is probably its due to its stronger visible light-harvesting ability.

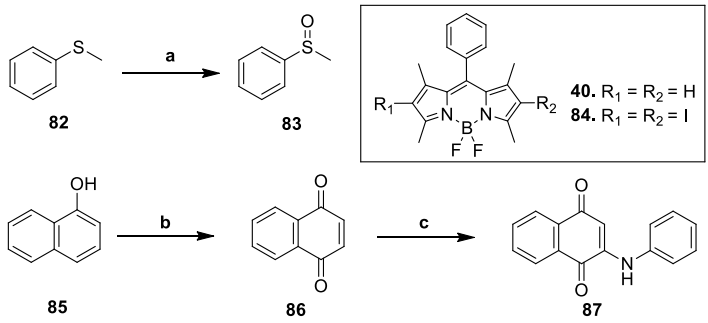

Scheme 7. **a 40/84**, visible light, air, CH_3OH; **b 84** (2 mol %), visible light, air, CH_2Cl_2/CH_3OH, 20 °C; **c** aniline, copper acetate, acetic acid, 65 °C, 3 h

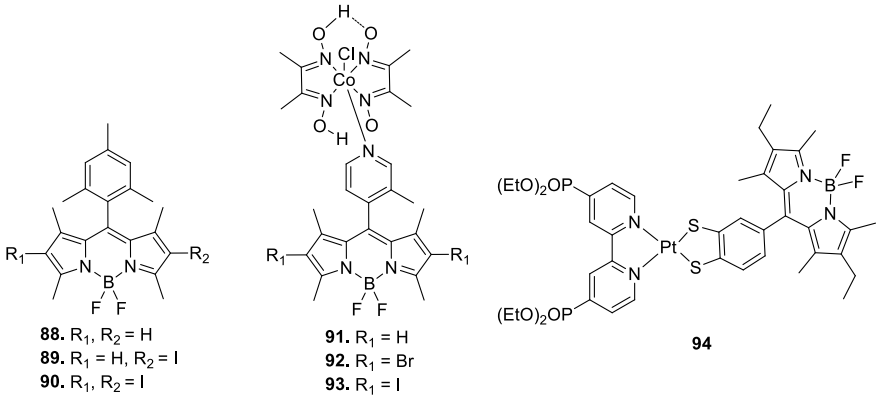

Fig. 13.18 Chemical structures of BODIPY based photocatalyst for hydrogen generation from water

BODIPY dyes are very efficient in catalyzing the hydrogen generation from water using visible light as energy source and converting it into chemical energy. In this system, BODIPY dyes act as photosensitisers (PSs) to harvest light energy and then transfer this energy into electrochemical energy by transferring electrons to a water reduction catalyst (WRC) to catalyze the proton reduction step.

Beweries et al. showed application of BODIPY dyes (**88–90**) (Fig. 13.18) as photosensitizers useful for light-driven hydrogen production in a multicomponent catalyst system comprising of BODIPY dye, bis(dichlorotriphenylphosphinppalladium) $[74]_2$, H_2O and trimethylamine (Dura et al. 2015). The dye **88** is capable of H_2 generation and its activity was further increased by iodination at the BODIPY dyes. Iodination enhances the triplet conversion as well as increases triplet lifetime of **89** and **90** which are essential for the intermolecular electron transfer.

Weare et al. showed the photocatalytic activity of BODIPY—cobaloxime complexes (**91–93**) (Fig. 13.18) for light-driven hydrogen evolution by proton reduction (Bartelmess et al. 2014). The triplet state of the BODIPY chromophores is required to transfer the electron to cobaloxime catalyst to show the catalytic activity. Thus, non-halogenated BODIPY—cobaloxime complex (**91**) was ineffective in hydrogen evolution. As the halogenation enhances the triplet state of BODIPY dyes, the hydrogen evolution efficiency of the complexes also increased with halogenation of BODIPY (**92**, **93**). Also the diiodo BODIPY—cobaloxime complex (**93**) was more efficient than the corresponding dibromo BODIPY—cobaloxime complex (**92**).

Eisenberg et al. developed dyad **94** comprising of BODIPY and platinum diimine dithiolate (PtN_2S_2) charge transfer (CT) chromophore which is very efficient in light driven hydrogen generation from aqueous protons (Fig. 13.18) (Zheng et al. 2015). This was attached with the TiO_2 nanoparticle through the attached $PO(OEt)_2$ groups for rapid electron photoinjection into the semiconductor. The dye on photoexciataion at 530 nm in water with ascorbic acid as electron donor, exhibited excellent H_2

production by generating ~40,000 turnover numbers of H_2 over 12 d (with respect to dye).

13.6 Conclusions

Thus, BODIPY is a class of dyes with outstanding optical as well as electrical properties. Synthetic versatility of these dyes showed that their properties can be modulated as per the requirement of different applications. All these attract scientists from almost every discipline of science to utilize these dyes for multiple applications in chemistry, biology, physics, materials science etc. Rational design of BODIPY dyes tuning their properties to develop custom made materials for different applications are discussed in this chapter. Several other applications of these dyes could not be incorporated here. The popularity of the BODIPY dyes among the scientific community clearly established them a unique dye for versatile optical applications.

But, still there are some lacuna/unfulfillment in different fields which need to be addressed in future. Several BODIPY dyes with high lasing efficiency are available from green-yellow-red to far red region. But low photostability is still a bottleneck for their continuous lasing applications. More focused studies are required to enhance their lasing lifetime. Efforts also need to develop water soluble BODIPY laser dyes for easy and safe operation. Similarly, development of high intensity and photostable BODIPY-based probes for single-molecule imaging and super-resolution microscopy is also required to visualize and analyze the localization and dynamics of individual proteins and biomolecules. Water solubility and aggregation of the BODIPY dyes in polar environment still remain a major problem for their applications in cellular imaging and photodynamic therapy of cancers. Despite many highly efficient BODIPY based triplet photosensitizers, they are still far from clinical applications as PDT agents. Priority research should be done to develop cancer cell specific BODIPY dyes targeting the over-expressed cell-surface receptors in tumor cells. Similarly, BODIPY based fluorescent-PET probes are still in the initial stages which need to develop. This can change the present cancer diagnosis and therapeutic scenario.

Numerous chemo/bio-sensor are reported, but water solubility, specificity of the sensors can be further improved for precise applications. Although abundant cation (metal) sensors are reported but sensors to detect quantify physiologically important anions in an aqueous environment are still lacking. BODIPY based photovoltaics showed good promise for future energy conversion devices. Dedicated research is needed to develop commercial small molecules based organic photovoltaics to fulfill the dream of the material chemists. Future development in all these areas will definitely happen as BODIPY class of dyes have all the required properties for these advancement which will further solidify their uniqueness in the world of fluorescent dyes.

References

Atilgan, S., Ekmekci, Z., Dogan, A.L., Guc, D., Akkaya, E.U.: Chem. Commun. 4398–4400 (2006)

Bartelmess, J., Francis, A.J., El Roz, K.A., Castellano, F.N., Weare, W.W., Sommer, R.D.: Inorg. Chem. **53**, 4527–4534 (2014)

Belmonte-Vázquez, J.L., Avellanal-Zaballa, E., Enríquez-Palacios, E., Cerdán, L., Esnal, I., Bañuelos, J., Villegas-Gómez, C., Arbeloa, I.L., Peña-Cabrera, E.: J. Org. Chem. **84**, 2523–2541 (2019)

Bessette, A., Hanan, G.S.: Chem. Soc. Rev. **43**, 3342–3405 (2014)

Bodio, E., Goze, C.: Dyes Pigm. **160**, 700–710 (2019)

Boens, N., Leen, V., Dehaen, W.: Chem. Soc. Rev. **41**, 1130–1172 (2012)

Boyer, J.H., Haag, A.M., Sathyamoorthi, G., Soong, M.-L., Thangaraj, K., Pavlopoulos, T.G.: Heteroat. Chem. **4**, 39–49 (1993)

Brown, S.B., Brown, E.A., Walker, I.: Lancet Oncol. **5**, 497–508 (2004)

Bulut, I., Huaulmé, Q., Mirloup, A., Chávez, P., Fall, S., Hébraud, A., Méry, S., Heinrich, B., Heiser, T., Lévêque, P., Leclerc, N.: Chemsuschem **10**, 1878–1882 (2017)

Buyukcakir, O., Bozdemir, O.A., Kolemen, S., Erbas, S., Akkaya, E.U.: Org. Lett. **11**, 4644–4647 (2009)

Cakmak, Y., Kolemen, S., Duman, S., Dede, Y., Dolen, Y., Kilic, B., Kostereli, Z., Yildirim, L.T., Dogan, A.L., Guc, D., Akkaya, E.U.: Angew. Chem. Int. Ed. **50**, 11937–11941 (2011)

Carlucci, G., Carney, B., Brand, C., Kossatz, S., Irwin, C.P., Carlin, S.D., Keliher, E.J., Weber, W., Reiner, T.: Mol. Imaging Biol. **17**, 848–855 (2015)

Dodani, S.C., He, Q., Chang, C.J.: J. Am. Chem. Soc. **131**, 18020–18021 (2009)

Dura, L., Ahrens, J., Pohl, M.-M., Höfler, S., Bröring, M., Beweries, T.: Chem. Eur. J. **21**, 13549–13552 (2015)

Er, J.C., Tang, M.K., Chia, C.G., Liew, H., Vendrell, M., Chang, Y.-T.: Chem. Sci. **4**, 2168–2176 (2013)

Ethirajan, M., Chen, Y., Joshi, P., Pandey, R.K.: Chem. Soc. Rev. **40**, 340–362 (2011)

Gabe, Y., Urano, Y., Kikuchi, K., Kojima, H., Nagano, T.: J. Am. Chem. Soc. **126**, 3357–3367 (2004)

Gorai, S., Ghosh, A., Chakraborty, S., Retailleau, P., Ghanty, T.K., Patro, B.S., Mula, S.: Dyes Pigm. **203**, 110343 (2022)

Gorman, A., Killoran, J., O'Shea, C., Kenna, T., Gallagher, W.M., O'Shea, D.F.: J. Am. Chem. Soc. **126**, 10619–10631 (2004)

Gupta, M., Mula, S., Tyagi, M., Ghanty, T.K., Murudkar, S., Ray, A.K., Chattopadhyay, S.: Chem. Eur. J. **19**, 17766–17772 (2013)

Gupta, M., Mula, S., Ghanty, T.K., Naik, D.B., Ray, A.K., Sharma, A., Chattopadhyay, S.: J. Photochem. Photobiol Chem. **349**, 162–170 (2017)

Harriman, A., Mallon, L.J., Elliot, K.J., Haefele, A., Ulrich, G., Ziessel, R.: J. Am. Chem. Soc. **131**, 13375–13386 (2009)

Hendricks, J.A., Keliher, E.J., Wan, D., Hilderbrand, S.A., Weissleder, R., Mazitschek, R.: Angew. Chem. Int. Ed. **51**, 4603–4606 (2012)

https://www.photonicsolutions.co.uk

Huang, L., Zhao, J., Guo, S., Zhang, C., Ma, J.: J. Org. Chem. **78**, 5627–5637 (2013)

Jagtap, K.K., Shivran, N., Mula, S., Naik, D.B., Sarkar, S.K., Mukherjee, T., Maity, D.K., Ray, A.K.: Chem. Eur. J. **19**, 702–708 (2013)

Jia, M.-Y., Wang, Y., Liu, Y., Niu, L.-Y., Feng, L.: Biosens. Bioelectron. **85**, 515–521 (2016)

Jiang, N., Fan, J., Liu, T., Cao, J., Qiao, B., Wang, J., Gao, P., Peng, X.: Chem. Commun. **49**, 10620–10622 (2013)

Jiang, X.-D., Zhao, J., Li, Q., Sun, C.-L., Guan, J., Sun, G.-T., Xiao, L.-J.: Dyes Pigm. **125**, 136–141 (2016)

Jiao, L., Yu, C., Uppal, T., Liu, M., Li, Y., Zhou, Y., Hao, E., Hub, X., Vicente, M.G.H.: Org. Biomol. Chem. **8**, 2517–2519 (2010)

Kamkaew, A., Lim, S.H., Lee, H.B., Kiew, L.V., Chung, L.Y., Burgess, K.: Chem. Soc. Rev. **42**, 77–88 (2013)
Killoran, J., Allen, L., Gallagher, J.F., Gallagher, W.M., O′Shea, D.F.: Chem. Commun. 1862–1863 (2002)
Kim, H., Kim, K., Son, S.-H., Choi, J.Y., Lee, K.-H., Kim, B.-T., Byun, Y., Choe, Y.S.: ACS Chem. Neurosci. **10**, 1445–1451 (2019)
Kollmannsberger, M., Rurack, K., Resch-Genger, U., Daub, J.: J. Phys. Chem. A **102**, 10211–10220 (1998)
Li, W., Li, L., Xiao, H., Qi, R., Huang, Y., Xie, Z., Jing, X., Zhang, H.: RSC Adv. **3**, 13417–13421 (2013)
Loudet, A., Burgess, K.: Chem. Rev. **107**, 4891–4932 (2007)
Lu, H., Mack, J., Yang, Y., Shen, Z.: Chem. Soc. Rev. **43**, 4778–4823 (2014)
Lundrigan, T., Crawford, S.M., Cameron, T.S., Thompson, A.: Chem. Commun. **48**, 1003–1005 (2012)
Maity, A., Sarkar, A., Sil, A., BN, S.B., Patra, S.K.: New J. Chem. **41**, 2296–2308 (2017)
Mbatia, H.W., Kennedy, D.P., Camire, C.E., Incarvito, C.D., Burdette, S.C.: Eur. J. Inorg. Chem. **2010**, 5069–5078 (2010)
Mora, A.K., Murudkar, S., Shivran, N., Mula, S., Chattopadhyay, S., Nath, S.: Int. J. Biol. Macromol. **166**, 1121–1130 (2021)
More, A.B., Mula, S., Thakare, S., Sekar, N., Ray, A.K., Chattopadhyay, S.: J. Org. Chem. **79**, 10981–10987 (2014)
More, A.B., Mula, S., Thakare, S., Chakraborty, S., Ray, A.K., Sekar, N., Chattopadhyay, S.: J. Lumin. **190**, 476–484 (2017)
Mula, S., Ray, A.K., Banerjee, M., Chaudhuri, T., Dasgupta, K., Chattopadhyay, S.: J. Org. Chem. **73**, 2146–2154 (2008)
Mula, S., Ulrich, G., Ziessel, R.: Tetrahedron Lett. **50**, 6383–6388 (2009)
Mula, S., Elliott, K., Harriman, A., Ziessel, R.: J. Phys. Chem. A **114**, 10515–10522 (2010)
Mula, S., Frein, S., Russo, V., Ulrich, G., Ziessel, R., Barberá, J., Deschenaux, R.: Chem. Mater. **27**, 2332–2342 (2015)
Nguyen, Q.T., Olson, E.S., Aguilera, T.A., Jiang, T., Scadeng, M., Ellies, L.G., Tsien, R.Y.: Proc. Natl. Acad. Sci. U S A **107**, 4317–4322 (2010)
Olivier, J.-H., Barberá, J., Bahaidarah, E., Harriman, A., Ziessel, R.: J. Am. Chem. Soc. **134**, 6100–6103 (2012)
Ortiz, M.J., Agarrabeitia, A.R., Duran-Sampedro, G., Bañuelos Prieto, J., Lopez, T.A., Massad, W.A., Montejano, H.A., García, N.A., Arbeloa, I.L.: Tetrahedron **68**, 1153–1162 (2012)
Quan, L., Gu, J., Lin, W., Wei, Y., Lin, Y., Liu, L., Ding, H., Pan, C., Xie, Z., Wu, T.: Chem. Commun. **55**, 8564–8566 (2019)
Ray, A.K., Kundu, S., Sasikumar, S., Rao, C.S., Mula, S., Sinha, S., Dasgupta, K.: Appl. Phys. B **87**, 483–488 (2007)
Ray, C., Schad, C., Moreno, F., Maroto, B.L., Bañuelos, J., Arbeloa, T., García-Moreno, I., Villafuerte, C., Muller, G., de la Moya, S.: J. Org. Chem. **85**, 4594–4601 (2020)
Sen, A., Mora, A.K., Koli, M., Mula, S., Kundu, S., Nath, S.: Int. J. Biol. Macromol. **220**, 901–909 (2022)
Shah, M., Thangaraj, K., Soong, M.-L., Wolford, L.T., Boyer, J.H., Politzer, I.R., Pavlopoulos, T.G.: Heteroat. Chem. **1**, 389–399 (1990)
Shivran, N., Mula, S., Ghanty, T.K., Chattopadhyay, S.: Org. Lett. **13**, 5870–5873 (2011)
Shivran, N., Tyagi, M., Mula, S., Gupta, P., Saha, B., Patro, B.S., Chattopadhyay, S.: Eur. J. Med. Chem. **122**, 352–365 (2016)
Shivran, N., Koli, M.R., Chakraborty, G., Srivastava, A.P., Chattopadhyay, S., Mula, S.: Org. Biomol. Chem. **19**, 7920–7929 (2021)
Srinivasa Rao, R., Bagui, A., Hanumantha Rao, G., Gupta, V., Singh, S.P.: Chem. Commun. **53**, 6953–6956 (2017)
Treibs, A., Kreuzer, F.-H.: Justus Liebigs Ann. Chem. **718**, 208–223 (1968)

Tsien, R.Y.: Nat. Rev. Mol. Cell Biol. Suppl. Ss16–21 (2003)
Turksoy, A., Yildiz, D., Akkaya, E.U.: Coord. Chem. Rev. **379**, 47–64 (2019)
Ulrich, G., Ziessel, R., Harriman, A.: Angew. Chem. Int. Ed. **47**, 1184–1201 (2008)
Valeur, B., Berberan-Santos, M.N.: Molecular Fluorescence: Principles and Applications, 2nd edn. Wiley-VCH Verlag GmbH & Co, KGaA (2012)
Wagner, R.W., Lindsey, J.S.: Pure Appl. Chem. **68**, 1373–1380 (1996)
Wainwright, M.: Chem. Soc. Rev. **25**, 351–359 (1996)
Wang, L., Xiao, Y., Tian, W., Deng, L.: J. Am. Chem. Soc. **135**, 2903–2906 (2013)
Wang, J.-L., Zhang, L., Gao, L.-X., Chen, J.-L., Zhou, T., Liu, Y., Jiang, F.-L.: J Mater Chem B **9**, 8639–8645 (2021)
Yang, Z., He, Y., Lee, J.-H., Park, N., Suh, M., Chae, W.-S., Cao, J., Peng, X., Jung, H., Kang, C., Kim, J.S.: J. Am. Chem. Soc. **135**, 9181–9185 (2013)
Yogo, T., Urano, Y., Ishitsuka, Y., Maniwa, F., Nagano, T.: J. Am. Chem. Soc. **127**, 12162–12163 (2005)
Zhang, X., Yu, H., Xiao, Y.: J. Org. Chem. **77**, 669–673 (2012)
Zhang, S., Wu, T., Fan, J., Li, Z., Jiang, N., Wang, J., Dou, B., Sun, S., Song, F., Peng, X.: Org. Biomol. Chem. **11**, 555–558 (2013)
Zhang, H.-X., Chen, J.-B., Guo, X.-F., Wang, H., Zhang, H.-S.: Anal. Chem. **86**, 3115–3123 (2014)
Zhang, D., Martín, V., García-Moreno, I., Costela, A., Pérez-Ojeda, M.E., Xiao, Y.: Chem. Chem. Phys. **13**, 13026–13033 (2011)
Zheng, B., Sabatini, R.P., Fu, W.F., Eum, M.S., Brennessel, W.W., Wang, L., McCamant, D.W., Eisenberg, R.: Proc. Natl. Acad. Sci. U S A **112**, E3987–E3996 (2015)
Ziessel, R., Ulrich, G., Harriman, A., Alamiry, M.A.H., Stewart, B., Retailleau, P.: Chem. Eur. J. **15**, 1359–1369 (2009)